China and India lead in greening of the world through land-use management

Chi Chen [1]*, Taejin Park[1], Xuhui Wang[2], Shilong Piao [2], Baodong Xu[1,3], Rajiv K. Chaturvedi[4], Richard Fuchs [5], Victor Brovkin [6], Philippe Ciais[7], Rasmus Fensholt [8], Hans Tømmervik[9], Govindasamy Bala[10], Zaichun Zhu [11], Ramakrishna R. Nemani[12] and Ranga B. Myneni[1]

Satellite data show increasing leaf area of vegetation due to direct factors (human land-use management) and indirect factors (such as climate change, CO_2 fertilization, nitrogen deposition and recovery from natural disturbances). Among these, climate change and CO_2 fertilization effects seem to be the dominant drivers. However, recent satellite data (2000–2017) reveal a greening pattern that is strikingly prominent in China and India and overlaps with croplands world-wide. China alone accounts for 25% of the global net increase in leaf area with only 6.6% of global vegetated area. The greening in China is from forests (42%) and croplands (32%), but in India is mostly from croplands (82%) with minor contribution from forests (4.4%). China is engineering ambitious programmes to conserve and expand forests with the goal of mitigating land degradation, air pollution and climate change. Food production in China and India has increased by over 35% since 2000 mostly owing to an increase in harvested area through multiple cropping facilitated by fertilizer use and surface- and/or groundwater irrigation. Our results indicate that the direct factor is a key driver of the 'Greening Earth', accounting for over a third, and probably more, of the observed net increase in green leaf area. They highlight the need for a realistic representation of human land-use practices in Earth system models.

The green leaves of vegetation sustain life on Earth by synthesizing sugars from water and CO_2 using the energy of sunlight and cool the surface by transpiring large amounts of water during this process. Their abundance is measured as the one-sided leaf area in broadleaf species and one-half the total needle surface area in coniferous species[1]. This varies seasonally between a maximum of $231 \times 10^6 km^2$ in July, when the Northern Hemisphere is at its greenest, and a minimum of $132 \times 10^6 km^2$ in January. The yearly average of $171 \times 10^6 km^2$ of leaf area found in $109 \times 10^6 km^2$ of vegetated area represents the annual average leaf area index (LAI) of the Earth—which is 1.57. Greening and browning are defined as statistically significant increases and decreases, respectively, in the annual average green leaf area at a location over a period of several years. Greening or browning could result from changes in the average leaf size, number of leafs per plant, the density of plants, the species composition, duration of green-leaf presence owing to changes in the growing season and multiple cropping.

Data from satellites, available since the early 1980s, indicate increasing greenness over the Earth's lands, from Svalbard to Australia and from Alaska to Chukotka[2–7]. The previously inferred dominant role of a CO_2 fertilization effect[7–11], and of indirect drivers in general[2,7,12–17], in the greening of the Earth raises the question of the role of human land use in shaping the vegetation greenness patterns on global lands. It may be more important than currently thought, for the following reasons. First, the models used in previous attribution analyses had rudimentary representations of evolving complex patterns of land-use practices (described below and elsewhere[18]), thus downplaying the direct role of humans in greening[19]. Second, the effects of higher CO_2 concentrations on plant growth[20], outside of experimental situations, are poorly understood and—as a consequence—the models differ widely in their prognostications[21]. Third, deleterious effects of the loss of sensor calibration, orbital drift of satellites, atmospheric contamination of vegetation signals and disjointed stitching of data from multiple sequential sensors were evident in the underlying satellite data[22] that were used in nearly all previous studies. Fourth, a recent study has shown that human land use is the dominant factor behind changes in woody and herbaceous vegetation cover[23]. Now that better quality leaf area data are available from the moderate resolution imaging spectroradiometer (MODIS) sensor observations[1,24–26]—Supplementary Table 1 describes the specifics of MODIS compared to advanced very high resolution radiometer (AVHRR) data—we aim here to assess the role of the direct driver, that is, human land-use management, without recourse to models, by characterizing the greening patterns in ecosystems globally.

Results

The Earth is greening. According to MODIS data, one-third of the global vegetated area is greening and 5% is browning. This translates to a net increase in leaf area of 2.3% per decade (Fig. 1 and

---

[1]Department of Earth and Environment, Boston University, Boston, MA, USA. [2]Sino-French Institute for Earth System Science, College of Urban and Environmental Sciences, Peking University, Beijing, China. [3]Macro Agriculture Research Institute, College of Resource and Environment, Huazhong Agricultural University, Wuhan, China. [4]Department of Humanities and Social Sciences, Birla Institute of Technology and Science, Pilani, Goa, India. [5]Institute of Meteorology and Climate Research—Atmospheric Environmental Research, Karlsruhe Institute of Technology, Garmisch-Partenkirchen, Germany. [6]Max Planck Institute for Meteorology, Hamburg, Germany. [7]Laboratoire des Sciences du Climat et de l'Environnement/IPSL, CEA-CNRS-UVSQ, Université Paris Saclay, Gif-sur-Yvette, France. [8]Department of Geosciences and Natural Resource Management, University of Copenhagen, Copenhagen, Denmark. [9]Norwegian Institute for Nature Research, Fram Centre, Tromsø, Norway. [10]Center for Atmospheric and Oceanic Sciences, Indian Institute of Science, Bangalore, India. [11]Shenzhen Key Laboratory of Circular Economy, Shenzhen Graduate School, Peking University, Shenzhen, China. [12]NASA Ames Research Center, Moffett Field, CA, USA. *e-mail: chenchi@bu.edu
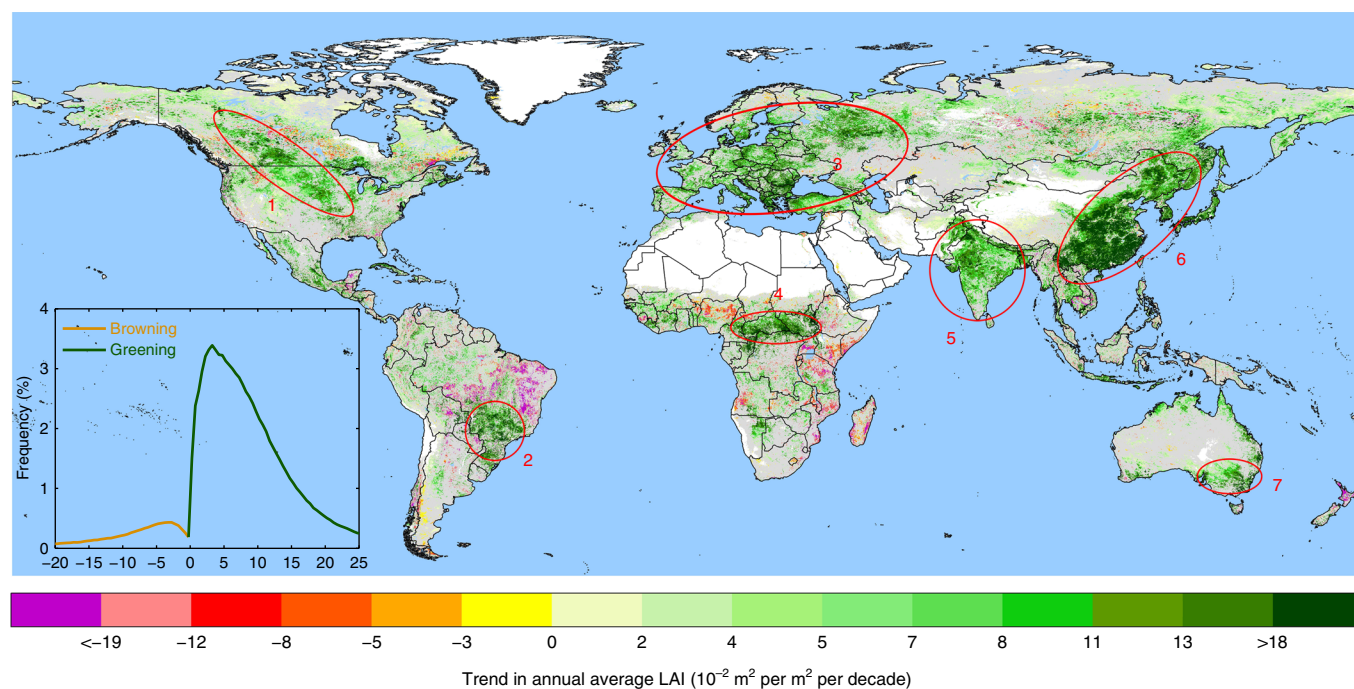
Fig. 1 | Map of trends in annual average MODIS LAI for 2000–2017. Statistically significant trends (Mann–Kendall test, $P \leq 0.1$) are colour-coded. Grey areas show vegetated land with statistically insignificant trends. White areas depict barren lands, permanent ice-covered areas, permanent wetlands and built-up areas. Blue areas represent water. The inset shows the frequency distribution of statistically significant trends. The highlighted greening areas in red circles mostly overlap with croplands, with the exception of circle number 4. Similar patterns are seen at $P \leq 0.05$ and the seven greening clusters are visible even at $P \leq 0.01$.

Table 1 | Net changes in leaf area (10^{-1} million km²) for the period 2000–2017

	Forests	Other woody vegetation	Grasslands	Croplands	All vegetation
Global	16.72	11.50	7.85	17.85	53.91
By latitude					
>50° S or N	4.78	3.48	0.80	2.36	11.41
25° S–50° S and 25° N–50°N	8.87	3.38	4.61	10.76	27.62
25° S–25° N	3.08	4.64	2.44	4.73	14.88
By MAT					
MAT <10 °C	7.48	3.61	4.04	5.23	20.36
MAT = 10–25 °C	7.92	5.82	2.46	7.70	23.89
MAT >25°C	1.32	2.06	1.35	4.92	9.65
By ATP					
ATP <500 mm	1.76	4.08	3.86	2.66	12.35
ATP = 500–1,000 mm	7.37	2.29	1.30	9.23	20.20
ATP >1,000 mm	7.59	5.13	2.69	5.95	21.35

Net changes were calculated as the difference between greening and browning for the period 2000–2017.

Supplementary Table 2), which is equivalent to adding 5.4×10^6 km² of new leaf area over the 18-year period of the record (2000 to 2017; Table 1). Two-thirds of this greening is from croplands and forests in about equal measure (Supplementary Table 3). The greening is prominently clustered in seven regions across six continents—most notably in China and India (Fig. 1), which together account for nearly one-third of the observed total net increase in green leaf area globally (China 25% and India 6.8%, Tables 1 and 2). This greening is seen over 65% of the vegetated lands in the two countries (Supplementary Table 4).

We compare the above results to those from AVHRR data[7], which we have recently updated using the same method described previously[27], for completeness. AVHRR data from the comparable period (2000–2016) show less greening (22% of vegetated lands) and more browning (14%) (Supplementary Table 2). Nearly 60% of the net increase in leaf area is from croplands, whereas forests show a net decrease (Supplementary Table 3). Of the seven greening clusters in MODIS (Fig. 1), six approximately match to the AVHRR data, albeit with lower spatial extents and weaker magnitudes, and the sub-Saharan cluster is missing from the AVHRR analysis

Table 2 | Ranking of the 11 largest countries by leaf area and its change during 2000–2017

Rank	Annual average leaf area in 2000 (million km²)	Net change in leaf area (10^{-1} million km²)	Net change in leaf area (%)
1	Brazil (29.68)	China (13.51)	China (17.80)
2	Russia (12.36)	Russia (7.57)	India (11.10)
3	United States (8.93)	EU (4.02)	EU (7.78)
4	Indonesia (8.69)	India (3.65)	Canada (7.13)
5	DRC (8.50)	United States (3.59)	Russia (6.62)
6	China (7.64)	Canada (3.35)	Australia (5.62)
7	Canada (5.41)	Australia (2.83)	United States (4.55)
8	EU (5.23)	Brazil (1.12)	Mexico (4.07)
9	Australia (5.19)	Mexico (0.96)	Argentina (1.70)
10	India (3.33)	DRC (0.96)	Brazil (1.54)
11	Mexico (2.66)	Indonesia (0.51)	DRC (1.34)
12	Argentina (2.16)	Argentina (0.13)	Indonesia (0.83)

The following large countries were excluded because of unfavourable climatic conditions for vegetation growth: Algeria, Denmark (which includes Greenland), Kazakhstan and Saudi Arabia. The EU is included here, although it is not a country. DRC, Democratic Republic of the Congo.

Table 3 | Ranking of the 11 largest countries by vegetated land area and proportion of vegetated lands that show statistically significant trends

Rank	Vegetated land area (million km²)	Proportion of vegetated lands showing greening (%)	Proportion of vegetated lands showing browning (%)
1	Russia (16.04)	India (69.0)	Brazil (11.6)
2	United States (8.91)	China (65.6)	Indonesia (6.8)
3	Canada (8.47)	EU (51.4)	Argentina (6.7)
4	Brazil (8.31)	Canada (41.6)	Canada (5.7)
5	Australia (7.50)	Russia (38.0)	DRC (4.5)
6	China (7.19)	United States (33.3)	United States (2.9)
7	EU (4.22)	Mexico (28.4)	Russia (2.7)
8	India (2.94)	Brazil (25.6)	Mexico (2.4)
9	Argentina (2.57)	Australia (24.4)	China (1.3)
10	DRC (2.28)	DRC (23.7)	EU (1.3)
11	Mexico (1.88)	Indonesia (19.7)	Australia (0.8)
12	Indonesia (1.80)	Argentina (13.2)	India (0.8)

The following large countries were excluded because of unfavourable climatic conditions for vegetation growth: Algeria, Denmark (which includes Greenland), Kazakhstan and Saudi Arabia. The EU is included here, although it is not a country.

(Supplementary Fig. 1a). The data from the two sensors agree on the magnitude of greening in China and India (Supplementary Table 4), probably because of the lower base LAI values (Table 2), larger spatial extents of greening (66 and 69%, respectively; Table 3) and higher relative changes in leaf area (18 and 11%, respectively; Table 2). Globally, LAI trends from the two sensors agree over 61% of the vegetated area and the disagreement is mostly in tropical humid areas and at Northern high latitudes, where the quality of the AVHRR data is poor (Supplementary Fig. 3). The full AVHRR record (1982–2016) shows more greening (41%) and browning (11%) in comparison to the shorter MODIS record, and the patterns exhibit both similarities (red circles in Supplementary Fig. 1b) and important differences (blue circles). The two are not expected to be comparable, although both point to a Greening Earth[2–7]. These results are consistent with recent independent estimates of changes in woody and herbaceous cover[23].

Human land use is a dominant driver of the Greening Earth. The above results provide at least four arguments in favour of a greater role for a direct human driver than previously thought[2,7,12]. First, cropland greening contributes the most to the net increase in leaf area globally since 2000 (33%, Table 1). Six out of seven greening clusters (Fig. 1) overlap with the areal pattern of agricultural primary productivity that has previously been derived independently[28] (Supplementary Fig. 2). Cropland greening is mainly attributable to the direct driver, without discounting the minor but opposing[29,30] contributions of the indirect drivers (CO_2 fertilization has been reported to increase crop production, whereas climate change has been reported to increase or decrease crop yields depending on the location). The green revolution can be attributed to quick-growing hybrid cultivars, multiple cropping, irrigation, fertilizer use, pest control, better quality seeds, farm mechanization, credit availability and crop insurance programmes[31]. Second, the suggestion that the CO_2 fertilization effect on greening should be seen prominently in hot and arid environments, where water limits plant growth[9,20], is not apparent in our analysis. Overall, greening of natural vegetation from these regions (a mean annual temperature (MAT) greater than 25 °C of 13% and an annual total precipitation (ATP)

less than 500 mm of 27%) contributes much less than those from mild (MAT < 25 °C, 87%) and wet (ATP > 500 mm, 73%) climates (Table 1)—this is also true when Table 1 entries are adjusted for vegetated area in each climate class. Third, compared to indirect drivers, gains from cropland production in the northern temperate regions, which overlap with the greening patterns presented here (Table 1), contribute more toward explaining the increasing amplitude of the seasonal cycle of atmospheric CO_2 concentration[32]. Finally, the large contribution of northern temperate forests to global net greening (16%, Table 1) indicates that large-scale tree plantations in previously low-productive areas of China and silvicultural practices in developed countries are important, further highlighting the role of the direct driver.

To further appreciate the importance of human land-use management in greening the world, we compare the trends in 11 large countries with sizeable populations and vegetated lands (Table 3). China and India stand out. They are the two most populous countries, but rank in the middle in terms of vegetated area. For this reason, and also because they are situated in temperate to subtropical climes, they rank either in the middle (China) or towards the bottom (India) in terms of annual average leaf area (Table 2). However, they rank at the top (and bottom) in terms of proportion of vegetated lands that exhibits greening (and browning; Table 3). As a consequence, they occupy the top ranks in terms of net increase in leaf area, both on an absolute and relative basis (Table 2). China alone accounts for 25% of the global net increase in leaf area with only 6.6% of global vegetated area. This is equal to the net greening in the three largest countries, Russia, the United States and Canada, that together hold 31% of the global vegetated area (Tables 1–3). India is similarly noteworthy. It ranks first (and last) in terms of the proportion of vegetated area that exhibits greening (and browning; Table 3). With only 2.7% of the global vegetated area, India accounts for 6.8% of the global net increase in leaf area, which is equal to that in the United States or Canada, each of which has three times more vegetated area. This statistic is even more remarkable considering that the annual average leaf area of India is two to three times smaller than that of Canada and the United States, respectively (Tables 2 and 3).
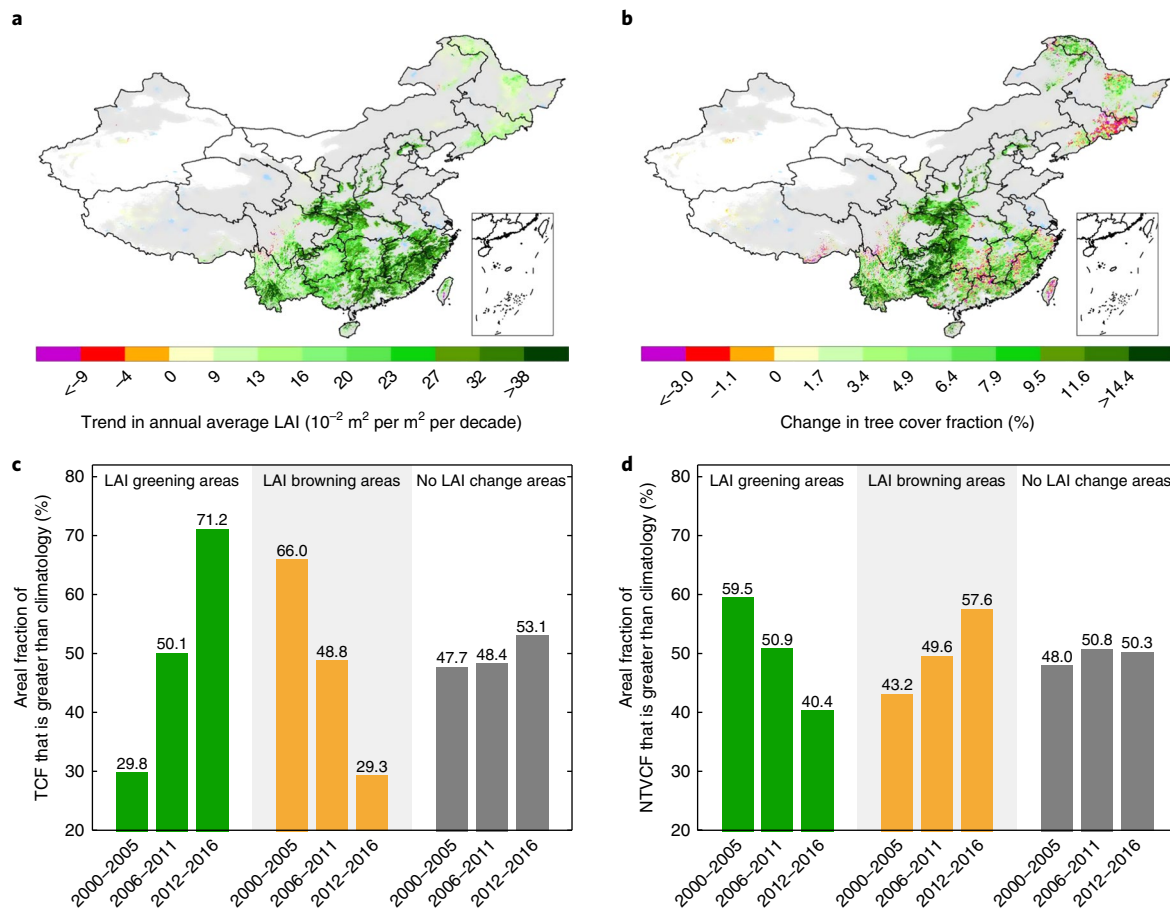
Fig. 2 | Trends in forests and other woody vegetation of China. a, Trend in annual average LAI of forests and other woody vegetation. **b**, Change in the fraction of tree cover in forests and areas of other woody vegetation between 2014–2016 and 2000–2002 in areas that show statistically significant LAI trends in **a**. Grey areas show vegetated land with statistically insignificant LAI trends or predominantly herbaceous vegetation. White areas depict land that is not vegetated. Black lines are boundaries of the first-level administrative divisions. **c,d**, Areal fraction of tree cover fraction (TCF) (**c**) and non-tree vegetation cover fraction (NTVCF) (**d**) over forests and other woody vegetation that is greater than the climatology during a particular period, that is, 2000–2005, 2006–2011 and 2012–2016. Climatology is the mean of values from long-term observations. The colours further confine the analysis to areas of LAI greening (green bars), browning (browning bars) and no LAI change (grey bars).

The European Union (EU) lands deserve a special mention in view of the prominent greening pattern in Fig. 1 (circle 3). This region, like China, ranks in the middle in terms of vegetated land area (Table 3) and average annual leaf area (Table 2) among the large countries studied here. Similar to China, it ranks at the top (third) in terms of vegetated lands that exhibit greening and towards the bottom for browning. These changes produce a top rank for this region for net increase in leaf area (third)—55% of which is due to croplands and 34% to forests (nearly all forests are managed in the EU). Recent studies traced the greening in European semi-natural vegetation to land-use practices, principally land abandonment and afforestation[33–35]. Brazil, on the other hand, ranks towards the bottom, because the greening from croplands and pastures is nearly offset by the browning of forests and cerrado[23]. The dominant cropland contribution to expansive greening in China, India, the EU and the United States, highlights the importance of the direct driver in global greening.

China and India lead in the greening of the Earth. We next investigated what factors explain the large-scale greening of China and India in the twenty-first century. Forests and croplands contribute 42% and 32%, respectively, to the net increase in leaf area of China whereas croplands alone contribute 82% in the case of India (the contribution of forests in India is minor, 4%, and was therefore not

discussed in detail). Focusing first on forested lands in China, we note an increase (or decrease) in tree (or non-tree) cover in the greening areas (84% of all forests and other wooded lands) and the opposite in the few (<1%) browning areas (Fig. 2). Forest inventories reveal a 19% increase in forest area ($330 \times 10^3 \text{km}^2$) in a single decade because of expanding natural forests and afforestation, in equal measures (Supplementary Table 5). China is implementing several ambitious programmes[36] to conserve and expand forests with the goal of mitigating soil erosion, air pollution and climate change (Supplementary Table 6). Already a third of the $2.08 \times 10^6 \text{km}^2$ of current forests are plantations (Supplementary Table 5) with rapidly growing young trees that are less than 40 years old[37]. For example, the mean LAI trend (0.23 m² per m² per decade) for regions with a planted forest fraction (PFF) ≥ 10% is 53% greater than the mean LAI trend (0.15 m² per m² per decade) for regions with PFF < 10%. Similarly, the mean tree cover trend (6.18% per decade) for regions with PFF ≥ 10% is 29% greater than the mean tree cover trend (4.90% per decade) for regions with PFF < 10%. Other recent studies attest to the success of these programmes in terms of ameliorating land degradation[38], lowering surface temperatures[39] and facilitating carbon sequestration[40], but a strain on water resources has also been noted[41]. All of this emphasizes the importance of human actions for the greening of the wooded lands of China.
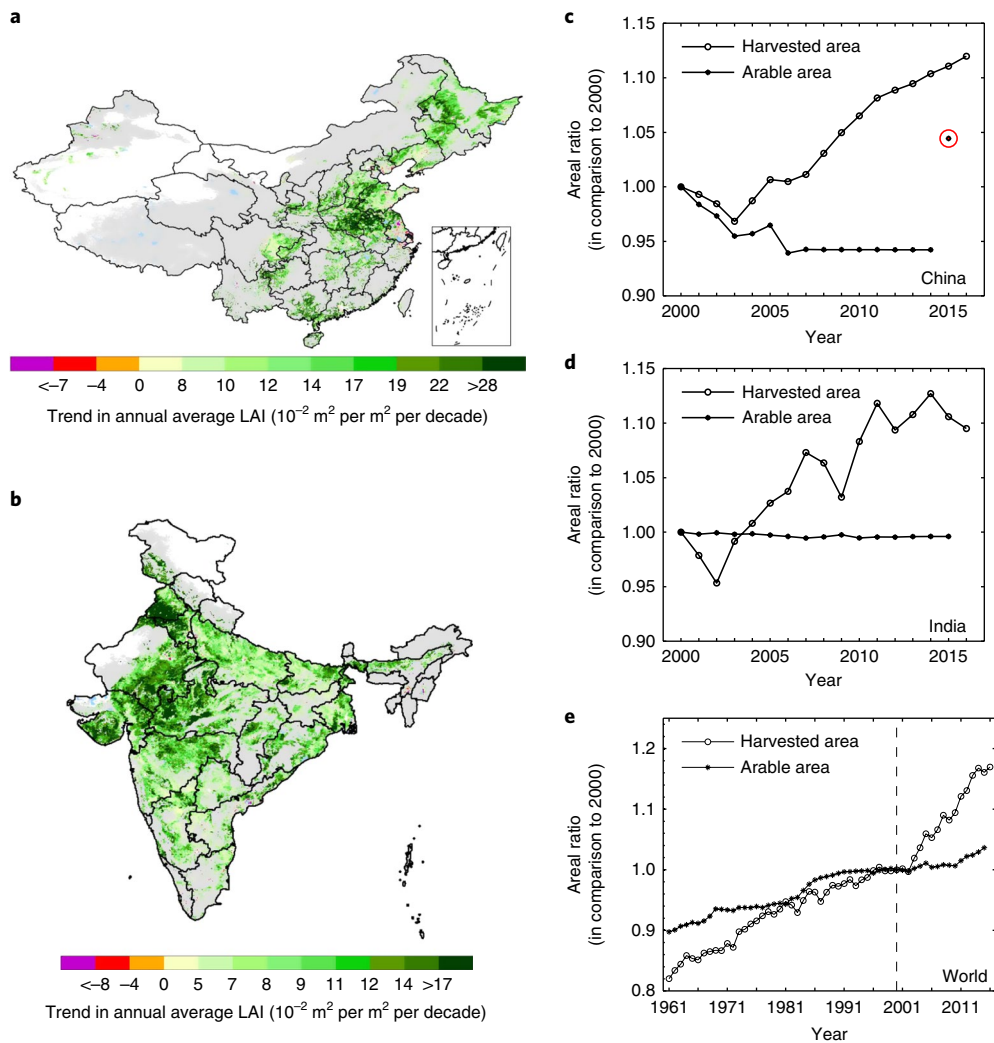
Fig. 3 | Leaf area trends in croplands of China and India. a,b, Trend in annual average LAI in croplands in China (**a**) and India (**b**). **c–e,** Ratio of harvested area (circle) and arable area (asterisk) with respect to 2000 values for China (**c**), India (**d**) and the world (**e**). The asterisk circled in red in **c** is an outlier. The vertical dash line in **e** indicates 2000.

A recent study[42] has reported browning trends in natural vegetation of India using MODIS normalized difference vegetation index (NDVI) data, but our reanalysis of the same data does not support this conclusion. The previous study[42] focused exclusively on the 8% and 4% browning proportions in forests and other woody vegetation classes while ignoring the 19% and 48% greening proportions in these two classes, during the period of their investigation (2001–2014; Supplementary Table 7). The greening proportions increase to 47% and 55% and the browning proportions decline to 1% and 0.5% for the full record (2000–2017). The browning during the shorter period (2001–2014) spans about 42,300 km² and is comparable to the previously published[42] estimate of 55,000 km². However, this decreases to 5,000 km² during the full record (2000–2017). Greening, on the other hand, is seven times greater (283,300 km²) during the shorter period and increases to being 80 times greater (401,800 km²) for the full record. An independent study[43] of trends in MODIS vegetation indices confirms our results.

With regards to cropland greening in China and India, we note that the two countries had comparable and stable land areas under crop cultivation since 2000 (about 1.92 and 2.11 × 10⁶ km², respectively, Fig. 3). Still, total food production (for example, grains, fruits and vegetables) has increased significantly (by 35% to 40%) according to our analysis of data from the Food and Agriculture

Organisation[44] ((FAO); Supplementary Table 8). For example, the total cereal production in China has increased by 43% from 407 × 10⁶ tonnes in 2000 to 583 × 10⁶ tonnes in 2016. Although yields in India are lower, total cereal production increased by 26% during the same period (from 235 to 295 × 10⁶ tonnes). This is largely because of the increase in harvested area through multiple cropping[45] (Fig. 3), which results in the observed greening trends. Agricultural intensification in China and India is being facilitated by heavy fertilizer use[46] and surface- and/or groundwater irrigation[47,48]—the two currently rank at the top for the amount of fertilizer use (Supplementary Table 7). Harvested land area at the global scale grew approximately four times faster than the cropland area since 2000 in large part due to these practices in China, India and Brazil[45] and this is reflected in the MODIS greening patterns (Fig. 1). Of particular interest is the leading and impressive relative changes in agricultural production, fertilizer use and harvested area in Brazil; however, this is due to starting from lower base values (Supplementary Table 8). The observed large-scale greening of China and India is a harbinger of food self-sufficiency for 2.7 billion people in the two top ranked countries in terms of agricultural output (nominal gross domestic product of US$1.1 and 0.41 trillion, respectively, in 2015 from the agricultural sector in 2015 according to the CIA World Factbook).

Concluding remarks. A third of the global vegetated lands are currently greening—that is, becoming more productive—in a pattern that is reflective of intensive human use of land for crops and forests across all continents, but most prominently in the two populous countries China and India. This suggests that human land-use management is an important driver of the Greening Earth[2–7], accounting for a third, and probably more, of the observed net increase in green leaf area. Therefore, one of the priorities for Earth System Model refinement is a realistic representation of the spatio-temporal dynamics of key land-use practices—multiple cropping, irrigation and fertilizer use, fallowing and abandonment of land, afforestation, reforestation and deforestation. Although human exploitation of land will remain a complex dynamic endeavour, monitoring this using spaceborne datasets, especially high-spatial-resolution data, may offer insights into how this may be realistically represented in models. Finally, it is important to note that the gain in greenness, which mostly occurred in the Northern temperate and high latitudes, does not offset the damage from loss of leaf area in tropical natural vegetation (for example, in Brazil, Democratic Republic of the Congo and Indonesia; Tables 2 and 3) and attendant consequences for ecosystem sustainability and biodiversity.

Methods

MODIS LAI product. Collection 6 (C6, also version 6) Terra and Aqua MODIS LAI products (MOD15A2H and MYD15A2H) are used in this study[49,50]. These LAI datasets are provided as 8-day composites with a 500-m sinusoidal projection covering the whole globe. They are further refined by rigorous checking of the quality flags of the LAI products and of the simultaneous vegetation index products, following the previously described methods[51]. This filtering provides the highest quality MODIS LAI observations that minimize any residual contamination from clouds, aerosols, snow and shadow. The two LAI datasets (that is, four 8-day composites) are then combined into a 16-day composite by taking the mean of all valid LAIs (temporal average). They are then spatially aggregated to generate 0.05° data in a climate-modelling grid ((CMG); the spatial average). The remaining gaps, although very few, are filled using the climatology of each 16-day composite during 2000–2017. Finally, the annual average LAI for each 0.05° pixel is calculated and used in this study.

The quality of C6 MODIS LAI datasets was comprehensively evaluated against ground-based measurements of LAI and through intercomparisons with other satellite LAI products[24,25]. These datasets represent the latest and highest quality LAI products that are currently available. They result from two decades of research on the LAI algorithm development, testing, refinement and validation—these efforts are described in over 50 peer-reviewed journal articles listed at the MODIS Land validation website[52].

AVHRR LAI3g product. We generated a new version of the LAI data (LAI3gV1) as part of this study based on the previously described methodology[27]. It has global coverage with bimonthly frequency and has a 1/12° spatial resolution. It spans the period July 1981 to December 2016. It is the longest among current LAI datasets. The full time series of LAI3gV1 data was generated by an artificial neural network algorithm that was trained with the overlapping data (2000–2016) of NDVI3gV1 and C6 Terra MODIS LAI datasets. Here, NDVI3gV1 refers to the new version of the third-generation normalized difference vegetation index data provided by Global Inventory Modeling and Mapping Studies (GIMMS) AVHRR[53]. The annual average of LAI3gV1 is calculated from 24 observations per year.

AVHRR LAI data prior to 2000 are not evaluated as required field data are not available. Ground data collected as part of MODIS validation efforts after 2000 were used to test the quality of AVHRR LAI data and these have been described previously[27].

MODIS land cover type product. The land cover information is provided by the collection 5.1 MODIS yearly product known as MCD12C1[54]. The spatial resolution of land cover is 0.05° in CMG. The International Geosphere-Biosphere Programme (IGBP) classification types provided by MCD12C1 are aggregated into four broad biome types in this study—forests, other woody vegetation, grasslands and croplands. Forests include evergreen needleleaf forest, evergreen broadleaf forest, deciduous needleleaf forest, deciduous broadleaf forest and mixed forest. Other woody vegetation includes closed shrublands, open shrublands and woody savannahs. Grasslands include savannahs and grasslands. Croplands include croplands and mosaics of croplands and natural vegetation. A static land cover map (that is the map for 2007) is used to define the above-mentioned four broad biome types.

MODIS vegetation continuous field product. C6 Terra MODIS vegetation continuous field is a yearly product that presents a continuous, subpixel fraction of land surface cover with a 250-m sinusoidal projection from 2000 to 2016[55].

The fraction of land surface cover has three components, which include the percentage of tree cover, percentage of non-tree vegetation cover and percentage of non-vegetated cover. The 250-m data are aggregated to 0.05° CMG in this study.

Temperature and precipitation data. Monthly 0.5° CMG temperature and precipitation data are provided by the University of East Anglia Climate Research Unit (CRU) and the latest version is CRU TS4.01[56]. MAT and ATP were calculated for each year. The climatology of the MAT and ATP is also evaluated during the period of 2000 to 2016. Three climatic zones were defined based on the climatology of MAT: (1) cool, MAT < 10 °C; (2) warm, MAT = 10–25 °C; and (3) hot, MAT > 25 °C. Another three climatic zones were defined based on the climatology of ATP: (1) dry, ATP < 500 mm; (2) wet, ATP = 500–1,000 mm; and (3) humid, ATP > 1,000 mm.

Data on country administrative areas. Data on country administrative areas was obtained from the Database of Global Administrative Areas (GADM) hosted by University of California at Davis (https://gadm.org/). The GADM data provide high-resolution shapefiles at all administrative levels, such as at the country, state or provincial level (https://gadm.org/). We used the latest version (v.2.8) in this study.

FAOSTAT database. Arable area, harvested area, cereal production and population were obtained from the FAOSTAT database hosted by the FAO[44]. Crop statistics (that is, arable area and harvested area) are recorded for 173 types of crops from 1961 to 2015/2016. Arable area and harvested area shown in Fig. 3 are ratios expressed relative to their corresponding values in year 2000. The 2017 population data given by FAO are estimated based on the 2015 Revision of World Population Prospects from the United Nations Population Division.

Forestry inventory data of China. The forestry inventory data of China is provided by the State Forestry Administration of China (http://www.forestry.gov.cn). We used forest statistics documented in the National Continuous Forest Inventory of China (1999–2003 and 2009–2013) to calculate the afforested area, and the changes in forest area and coverage. We also used the planted forest map of China at a 1-km spatial resolution, which was obtained from the Seventh National Forest Resource Inventory (2004–2008).

Calculation of LAI trends. Trends in annual average MODIS LAI (2000 to 2017) and AVHRR LAI3gV1 (1982 to 2016 and 2000 to 2016) are evaluated by the Mann–Kendall test, which is a non-parametric test to detect monotonic trend in time series data. We used the function 'zyp.trend.vector' with the Yue–Pilon pre-whitening method provided by R package 'zyp' to conduct the trend test[57]. The trends with $P \leq 0.1$ are considered to be statistically significant in this study. Similar patterns are seen at $P \leq 0.05$ and the seven greening clusters (Fig. 1) are visible even at $P \leq 0.01$.

Calculation of the net change in leaf area. Trends in annual average MODIS LAI were considered to be linear when we calculated net changes in the leaf area during the period from 2000 to 2017. The net changes in leaf area for a specific region take into account the effects from both statistically significant browning and greening areas, and set the areas with statistically insignificant trends to a zero contribution, as shown in equation (1):

$$\text{Net leaf area changes per region} = \sum\nolimits_{i=1}^{n} \text{Tr}_i A_i N_{yr} \tag{1}$$

where i represents a pixel with a statistically significant trend, n is the total number of such pixels in the region, Tr_i is the trend of a pixel, A_i is the area of a pixel that varies with latitudes, and N_{yr} is the length of the study period which is set to 17.

Growing season-integrated LAI and annual average LAI. The annual average LAI is used in our analyses, rather than a growing season-integrated LAI[7], as it is better suited for our global study, in which we aimed to emphasize the importance of land-use management, including different cropping cycles (single/multiple) and temporal changes. The annual average LAI has the advantage of being simple, can be evaluated for all regions of the globe, including those with multiple growing seasons, a year-long growing season in the tropical humid forests and when the growing season spans two calendar years. It does not suffer from certain limitations of growing season-integrated LAI, namely, the subjective use of thresholds to define the start and end dates of a growing season and interpolation of 16-day composite satellite data to a daily resolution[6].

Data availability

The datasets generated during and/or analysed in this study are publicly available as referenced within the article. All data and scripts are available from the corresponding author on request.

References

1. Myneni, R. B. et al. Global products of vegetation leaf area and fraction absorbed PAR from year one of MODIS data. *Remote Sens. Environ.* **83**, 214–231 (2002).

2. Myneni, R. B., Keeling, C. D., Tucker, C. J., Asrar, G. & Nemani, R. R. Increased plant growth in the northern high latitudes from 1981 to 1991. *Nature* **386**, 698–702 (1997).

3. Zhou, L. et al. Variations in northern vegetation activity inferred from satellite data of vegetation index during 1981 to 1999. *J. Geophys. Res.* **106**, 20069–20083 (2001).

4. Xu, L. et al. Temperature and vegetation seasonality diminishment over northern lands. *Nat. Clim. Change* **3**, 581–586 (2013).

5. Vickers, H. et al. Changes in greening in the high Arctic: insights from a 30 year AVHRR max NDVI dataset for Svalbard. *Environ. Res. Lett.* **11**, 105004 (2016).

6. Park, T. et al. Changes in growing season duration and productivity of northern vegetation inferred from long-term remote sensing data. *Environ. Res. Lett.* **11**, 084001–084012 (2016).

7. Zhu, Z. et al. Greening of the Earth and its drivers. *Nat. Clim. Change* **6**, 791–795 (2016).

8. Piao, S. et al. Detection and attribution of vegetation greening trend in China over the last 30 years. *Glob. Change Biol.* **21**, 1601–1609 (2015).

9. Donohue, R. J., Roderick, M. L., McVicar, T. R. & Farquhar, G. D. Impact of CO_2 fertilization on maximum foliage cover across the globe's warm, arid environments. *Geophys. Res. Lett.* **40**, 3031–3035 (2013).

10. Keenan, T. F. et al. Recent pause in the growth rate of atmospheric CO_2 due to enhanced terrestrial carbon uptake. *Nat. Commun.* **7**, 13428 (2016).

11. Cheng, L. et al. Recent increases in terrestrial carbon uptake at little cost to the water cycle. *Nat. Commun.* **8**, 110 (2017).

12. Nemani, R. R. et al. Climate-driven increases in global terrestrial net primary production from 1982 to 1999. *Science* **300**, 1560–1563 (2003).

13. Goetz, S. J., Bunn, A. G., Fiske, G. J. & Houghton, R. A. Satellite-observed photosynthetic trends across boreal North America associated with climate and fire disturbance. *Proc. Natl Acad. Sci. USA* **102**, 13521–13525 (2005).

14. Fensholt, R. et al. Greenness in semi-arid areas across the globe 1981–2007 — an Earth Observing Satellite based analysis of trends and drivers. *Remote Sens. Environ.* **121**, 144–158 (2012).

15. Forkel, M. et al. Enhanced seasonal CO_2 exchange caused by amplified plant productivity in northern ecosystems. *Science* **351**, 696–699 (2016).

16. Mao, J. et al. Human-induced greening of the northern extratropical land surface. *Nat. Clim. Change* **6**, 959–963 (2016).

17. Bjorkman, A. D. et al. Plant functional trait change across a warming tundra biome. *Nature* **562**, 57–62 (2018).

18. Prestele, R. et al. Current challenges of implementing anthropogenic land-use and land-cover change in models contributing to climate change assessments. *Earth Syst. Dynam.* **8**, 369–386 (2017).

19. Piao, S. et al. Lower land-use emissions responsible for increased net land carbon sink during the slow warming period. *Nat. Geosci.* **11**, 739–743 (2018).

20. McMurtrie, R. E. et al. Why is plant-growth response to elevated CO_2 amplified when water is limiting, but reduced when nitrogen is limiting? A growth-optimisation hypothesis. *Funct. Plant Biol.* **35**, 521–534 (2008).

21. Wenzel, S., Cox, P. M., Eyring, V. & Friedlingstein, P. Projected land photosynthesis constrained by changes in the seasonal cycle of atmospheric CO_2. *Nature* **538**, 499–501 (2016).

22. Tian, F. et al. Evaluating temporal consistency of long-term global NDVI datasets for trend analysis. *Remote Sens. Environ.* **163**, 326–340 (2015).

23. Song, X. P. et al. Global land change from 1982 to 2016. *Nature* **560**, 639–643 (2018).

24. Yan, K. et al. Evaluation of MODIS LAI/FPAR product Collection 6. Part 1: consistency and improvements. *Remote Sens.* **8**, 359 (2016).

25. Yan, K. et al. Evaluation of MODIS LAI/FPAR product Collection 6. Part 2: validation and intercomparison. *Remote Sens.* **8**, 460 (2016).

26. Knyazikhin, Y., Martonchik, J. V., Myneni, R. B., Diner, D. J. & Running, S. W. Synergistic algorithm for estimating vegetation canopy leaf area index and fraction of absorbed photosynthetically active radiation from MODIS and MISR data. *J. Geophys. Res.* **103**, 32257–32275 (1998).

27. Zhu, Z. et al. Global data sets of vegetation leaf area index (LAI)3g and fraction of photosynthetically active radiation (FPAR)3g derived from global inventory modeling and mapping studies (GIMMS) normalized difference vegetation index (NDVI3g) for the period 1981 to 2011. *Remote Sens.* **5**, 927–948 (2013).

28. Wolf, J. et al. Biogenic carbon fluxes from global agricultural production and consumption. *Global Biogeochem. Cycles* **29**, 1617–1639 (2015).

29. Lobell, D. B., Schlenker, W. & Costa-Roberts, J. Climate trends and global crop production since 1980. *Science* **333**, 616–620 (2011).

30. Rosenzweig, C. & Parry, M. L. Potential impact of climate change on world food supply. *Nature* **367**, 133–138 (1994).

31. Jain, H. K. *Green Revolution: History, Impact and Future* (Studium, Houston, 2010).

32. Zeng, N. et al. Agricultural Green Revolution as a driver of increasing atmospheric CO_2 seasonal amplitude. *Nature* **515**, 394–397 (2014).

33. Buitenwerf, R., Sandel, B., Normand, S., Mimet, A. & Svenning, J.-C. Land surface greening suggests vigorous woody regrowth throughout European semi-natural vegetation. *Global Change Biol.* **24**, 5789–5801 (2018).

34. Fuchs, R., Herold, M., Verburg, P. H., Clevers, J. G. P. W. & Eberle, J. Gross changes in reconstructions of historic land cover/use for Europe between 1900 and 2010. *Global Change Biol.* **21**, 299–313 (2015).

35. Fuchs, R. et al. Assessing the influence of historic net and gross land changes on the carbon fluxes of Europe. *Global Change Biol.* **22**, 2526–2539 (2016).

36. Zhang, Y. et al. Multiple afforestation programs accelerate the greenness in the 'Three North' region of China from 1982 to 2013. *Ecol. Indic.* **61**, 404–412 (2016).

37. Zhang, Y., Yao, Y., Wang, X., Liu, Y. & Piao, S. Mapping spatial distribution of forest age in China. *Earth Space Sci.* **4**, 108–116 (2017).

38. Tong, X. et al. Increased vegetation growth and carbon stock in China karst via ecological engineering. *Nat. Sustain.* **1**, 44–50 (2018).

39. Peng, S. S. et al. Afforestation in China cools local land surface temperature. *Proc. Natl Acad. Sci. USA* **111**, 2915–2919 (2014).

40. Lu, F. et al. Effects of national ecological restoration projects on carbon sequestration in China from 2001 to 2010. *Proc. Natl Acad. Sci. USA* **115**, 4039–4044 (2018).

41. Feng, X. et al. Revegetation in China's Loess Plateau is approaching sustainable water resource limits. *Nat. Clim. Change* **6**, 1019–1022 (2016).

42. Chakraborty, A., Seshasai, M. V. R., Reddy, C. S. & Dadhwal, V. K. Persistent negative changes in seasonal greenness over different forest types of India using MODIS time series NDVI data (2001–2014). *Ecol. Indic.* **85**, 887–903 (2018).

43. Zhang, Y., Song, C., Band, L. E., Sun, G. & Li, J. Reanalysis of global terrestrial vegetation trends from MODIS products: browning or greening? *Remote Sens. Environ.* **191**, 145–155 (2017).

44. *FAOSTAT Database* (FAO, 2018); http://www.fao.org/faostat/

45. Ray, D. K. & Foley, J. A. Increasing global crop harvest frequency: recent trends and future directions. *Environ. Res. Lett.* **8**, 044041 (2013).

46. Lu, C. & Tian, H. Global nitrogen and phosphorus fertilizer use for agriculture in the past half century: shifted hot spots and nutrient imbalance. *Earth Syst. Sci. Data* **9**, 181–192 (2017).

47. Mueller, N. D. et al. Closing yield gaps through nutrient and water management. *Nature* **490**, 254–257 (2012).

48. Ambika, A. K., Wardlow, B. & Mishra, V. Remotely sensed high resolution irrigated area mapping in India for 2000 to 2015. *Sci. Data* **3**, 160118 (2016).

49. Myneni, R., Knyazikhin Y. & Park, T. *MOD15A2H MODIS/Terra Leaf Area Index/FPAR 8-day L4 Global 500 m SIN Grid V006 Data Set* (NASA, 2015); https://doi.org/10.5067/MODIS/MOD15A2H.006

50. Myneni, R., Knyazikhin, Y. & Park, T. *MYD15A2H MODIS/Aqua Leaf Area Index/FPAR 8-day L4 Global 500 m SIN Grid V006 Data Set* (NASA, 2015); https://doi.org/10.5067/MODIS/MYD15A2H.006

51. Samanta, A. et al. Comment on "Drought-induced reduction in global terrestrial net primary production from 2000 through 2009". *Science* **333**, 1093 (2011).

52. MODIS land team. *Validation: Status for LAI/FPAR (MOD15)* (NASA, 2018); https://landval.gsfc.nasa.gov/ProductStatus.php?ProductID=MOD15

53. Pinzon, J. & Tucker, C. A non-stationary 1981–2012 AVHRR NDVI3g time series. *Remote Sens.* **6**, 6929–6960 (2014).

54. Friedl, M. A., McIver, D. K., Hodges, J. & Zhang, X. Y. Global land cover mapping from MODIS: algorithms and early results. *Remote Sens. Environ.* **83**, 287–302 (2002).

55. Dimiceli, C. et al. *MOD44B MODIS/Terra Vegetation Continuous Fields Yearly L3 Global 250 m SIN Grid V006 Data Set* (NASA, 2015); https://doi.org/10.5067/MODIS/MOD44B.006

56. Harris, I. C. & Jones, P. D. *CRU TS4.01: Climatic Research Unit (CRU) Time-Series (TS) version 4.01 of High-Resolution Gridded Data of Month-by-Month Variation in Climate (Jan. 1901–Dec. 2016)* (Centre for Environmental Data Analysis, 2017); https://doi.org/10.5285/58a8802721c94c66ae45c3baa4d814d0

57. Bronaugh, D. & Werner, A. zyp: Zhang + Yue-Pilon trends package. R package version 0.10-1 https://cran.r-project.org/web/packages/zyp/index.html (2013).

Author Contributions

C.C. carried out the analyses with contributions from T.P., X.W., B.X., R.K.C. and R.F. C.C. and R.B.M. wrote the article. All authors contributed ideas for analyses, comments and critiques on drafts.

Competing interests

The authors declare no competing interests.

Additional information

Supplementary information is available for this paper at https://doi.org/10.1038/s41893-019-0220-7.

Reprints and permissions information is available at www.nature.com/reprints.

Correspondence and requests for materials should be addressed to C.C.

Publisher's note: Springer Nature remains neutral with regard to jurisdictional claims in published maps and institutional affiliations.

© The Author(s), under exclusive licence to Springer Nature Limited 2019